



Experimental and theoretical analysis of a method to predict thermal runaway in Li-ion cells



Krishna Shah, Divya Chalise, Ankur Jain*

Mechanical and Aerospace Engineering Department, University of Texas at Arlington, Arlington, TX, USA

HIGHLIGHTS

- Derives a non-dimensional thermal parameter to predict thermal runaway.
- Experimental measurements are in good agreement with the model predictions.
- Predicts safe and unsafe regions of the thermal design space.
- Results may facilitate thermal management design for enhanced safety.

ARTICLE INFO

Article history:

Received 3 August 2016
Received in revised form
29 August 2016
Accepted 30 August 2016

Keywords:

Lithium ion battery
Safety
Thermal runaway
Battery cooling
Thermal modeling

ABSTRACT

Thermal runaway is a well-known safety concern in Li-ion cells. Methods to predict and prevent thermal runaway are critically needed for enhanced safety and performance. While much work has been done on understanding the kinetics of various heat generation processes during thermal runaway, relatively lesser work exists on understanding how heat removal from the cell influences thermal runaway. Through a unified analysis of heat generation and heat removal, this paper derives and experimentally validates a non-dimensional parameter whose value governs whether or not thermal runaway will occur in a Li-ion cell. This parameter is named the Thermal Runaway Number (*TRN*), and comprises contributions from thermal transport within and outside the cell, as well as the temperature dependence of heat generation rate. Experimental data using a 26650 thermal test cell are in good agreement with the model, and demonstrate the dependence of thermal runaway on various thermal transport and heat generation parameters. This parameter is used to predict the thermal design space in which the cell will or will not experience thermal runaway. By combining all thermal processes contributing to thermal runaway in a single parameter, this work contributes towards a unified understanding of thermal runaway, and provides the fundamental basis for design tools for safe, high-performance Li-ion batteries.

© 2016 Elsevier B.V. All rights reserved.

1. Introduction

Thermal runaway in Li-ion cells is a widely researched phenomenon that presents severe safety challenges [1–3] and often requires conservative design and run-time control of energy conversion and storage devices, resulting in reduced performance [4,5]. Fundamentally, thermal runaway in a Li-ion cell is a cascade of successive processes and reactions that feed into one another through heat generation that increases with temperature, eventually leading to explosion and fire [1,3]. Pertinent processes in thermal runaway include decomposition of the solid-electrolyte

interface [6], various chemical reactions involving the electrolyte and electrode binder [7–9], and eventually, decomposition of electrolyte [10] and positive electrode active material [11]. A large amount of literature is available on understanding each of these processes [1,3,6,7,12,13]. In particular, the reaction kinetics and heat generation profiles of these processes have been widely studied, both theoretically [12] and through experimental measurements using tools such as Differential Scanning Calorimetry (DSC) and Accelerated Rate Calorimetry (ARC) [6,7,13]. These processes are usually modeled using Arrhenius reaction kinetics, with a reaction rate, and hence heat generation rate, that increases exponentially with temperature [1,3]. Numerical values of these reaction rates and heat generation rates, as well as their temperature dependence have been determined [3]. Some work also exists on overall heat generation rate measurement from a Li-ion cell at large discharge

* Corresponding author. 500 W First St, Rm 211, Arlington, TX, 76019, USA.
E-mail address: jaina@uta.edu (A. Jain).

rates where thermal runaway may be a concern [14,15].

Some research has also been carried out on thermal modeling and measurements for Li-ion cells in thermal runaway situations [12,16–21]. Analytical methods and simulation tools [12,16–18] have been used for modeling thermal behavior of a cell at elevated temperatures. Experiments have been carried out to measure temperature of a cell or an appropriate thermal surrogate [19–21] during runaway. However, not much work has been carried out on connecting heat removal and heat generation processes that occur during thermal runaway. While heat generation is a function of the chemical reactions occurring within the cell, heat removal from the cell comprises of two processes that occur in series [22,23] – thermal conduction within the cell to its outside surface, and heat removal, usually through convection from the outside surface to the ambient. The nature of interaction between these heat generation and heat transfer processes eventually determines the thermal state of the cell, and whether thermal runaway occurs or not. It is critical to model both in a holistic fashion to better understand, and design means to prevent thermal runaway. Specifically, it is of interest to determine how the thermal transport properties of the cell and its ambient influence and govern the occurrence of thermal runaway. Such experimentally-verified theoretical limits on the occurrence or avoidance of thermal runaway may result in valuable design tools for safety of Li-ion cells.

The interaction between heat generation and heat removal has been represented in past papers in the form of a Semenov plot [24,25] that compares the rates of heat generation and heat removal as functions of the temperature of the cell. A Semenov plot uses the imbalance between the two processes – which increase exponentially and linearly respectively as functions of temperature – as the basis for predicting thermal runaway [24,25]. However, this approach assumes the cell to be a lumped thermal mass with uniform temperature throughout the cell volume. As shown by recent models [22,23] and measurements [26,27], this may not be an accurate assumption. As a consequence, the Semenov analysis predicts the thermal runaway process to be independent of the thermal conductivity of the cell, which is not accurate in several cases. For example, the Biot number [28] for a typical 26650 cell in natural convection conditions can be estimated to be 2–6.5 based on recent thermal conductivity measurements of the cell [29,30]. A value of $Bi > 1$ indicates strong temperature gradients within the cell, making the lumped mass based Semenov analysis inaccurate. Because the Semenov approach neglects heat transfer within the cell, it has not been possible so far to predict what internal and external thermal conditions are needed to prevent thermal runaway for a specific cell chemistry with well-known chemical kinetics and heat generation rates as functions of temperature. Accounting for this phenomenon will help optimize materials design from a thermal perspective, and help maintain a balance between internal and external heat transfer towards avoidance of thermal runaway.

This paper carries out theoretical and experimental analysis of thermal runaway in Li-ion cells by extending the Semenov analysis to account for heat transfer within the cell. The governing energy conservation equation that accounts for both heat generation and heat removal processes is solved to determine a non-dimensional parameter – which is named the Thermal Runaway Number (TRN) – whose value is shown to govern whether thermal runaway will occur or not. This parameter includes contributions from heat transfer processes within and outside the cell, as well as the rate of increase in heat generation with temperature. Results indicate that thermal conductivity within the cell is a critical thermal property governing runaway. Experiments that implement a temperature-dependent heat generation with a controllable temperature slope

are carried out to validate the theoretical model. These experimental data are in good agreement with theoretical results, and demonstrate successful avoidance of thermal runaway through changes in the convective heat transfer coefficient external to the cell. Design guidelines that predict the parameter space in which thermal runaway can be prevented are developed using the model. The experimentally-verified fundamental insights in this paper may lead to design guidelines for thermal properties of the cell and its ambient for prevention of thermal runaway.

2. Mathematical modeling

Consider a cylindrical Li-ion cell of radius R , radial thermal conductivity k_r , heat capacity C_p and mass density ρ . The cell experiences a temperature-dependent internal heat generation rate $Q(T)$ throughout its volume, and is being cooled at the outside surface with a convective heat transfer h due to a mechanism such as coolant flow. The interest is in determining the parameter space within which the cell will not undergo thermal runaway, i.e. the cell temperature does not become unbounded. In this case, the governing energy equation for the temperature rise $T(r,t)$ in the cell is given by

$$k_r \left(\frac{\partial^2 T}{\partial r^2} + \frac{1}{r} \frac{\partial T}{\partial r} \right) + Q(T) = \rho \cdot C_p \frac{\partial T}{\partial t} \quad (1)$$

subject to

$$\frac{\partial T}{\partial r} = 0 \quad \text{at } r = 0 \quad (2)$$

and

$$-k_r \left(\frac{\partial T}{\partial r} \right) = h \cdot T \quad \text{at } r = R \quad (3)$$

Equations (1)–(3) can be solved to determine if there is a set of conditions that will prevent thermal runaway by ensuring a bounded solution for T at all times. To do so, a Taylor series expansion of $Q(T)$ is first carried out about a temperature $T = T_0$, and second order and higher terms are neglected. This results in

$$k_r \left(\frac{\partial^2 T}{\partial r^2} + \frac{1}{r} \frac{\partial T}{\partial r} \right) + Q(T_0) + \beta(T - T_0) = \rho C_p \frac{\partial T}{\partial t} \quad (4)$$

where $\beta = \frac{dQ}{dT}$ is the slope of $Q(T)$.

In order to solve equation (4), it is noted that the heat generation term can be split linearly into two components, $(Q(T_0) - \beta T_0)$ and βT . The first component is a constant quantity, which from thermal conduction theory [31] is known to result in a steady state with a bounded temperature field. However, the second heat generation component βT increases with temperature, and may lead to an unbounded temperature. Solving only for $T_2(r,t)$, which represents the temperature rise due to the second component of heat generation, it can be shown using the technique of separation of variables [31] that

$$T_2(r, t) = \sum_{n=1}^{\infty} C_n J_0 \left(\frac{\mu_n r}{R} \right) \cdot \exp \left(\frac{k_r}{\rho \cdot C_p} \left(\frac{\beta}{k_r} - \frac{\mu_n^2}{R^2} \right) \cdot t \right) \quad (5)$$

where J_0 is the Bessel function of the first kind of order 0, C_n are constant coefficients, and μ_n are non-dimensional eigenvalues given by the roots of the equation

$$Bi \cdot J_0(x) - x J_1(x) = 0 \quad (6)$$

where $Bi = \frac{hR}{k_r}$ is the Biot number [28]. Note that C_n in equation (5) are obtained using orthogonality and the initial condition of the temperature field.

The temperature solution in equation (5) may be either bounded or unbounded depending on the sign of the term within the exponential function in equation (5). This term remains bounded if

$$\frac{\beta}{k_r} - \frac{\mu_n^2}{R^2} < 0 \quad (7)$$

for each $n = 1, 2, 3$.

Since the values of μ_n increase with n , it is sufficient to require that the first eigenvalue μ_1 satisfies equation (7). This condition can be written in terms of a single non-dimensional parameter as

$$TRN \equiv \frac{\beta \cdot R^2}{k_r \mu_1^2} < 1 \quad (8)$$

Thus, a fundamental, non-dimensional parameter has been derived, which we name as the Thermal Runaway Number (TRN), whose value must be less than one in order to prevent thermal runaway. Since this derivation is based on Taylor series expansion of $Q(T)$ at a specific temperature T_0 , therefore equation (8) must be satisfied over the entire temperature range of operation to ensure that thermal runaway does not occur throughout.

The non-dimensional parameter TRN in equation (8) is a combination of properties of thermal transport within the cell (k_r), thermal transport from the cell surface to the outside (μ_1) and the kinetics of heat generation (β), as well as the cell geometry (R). These parameters combined in the manner shown in equation (8) determine whether thermal runaway occurs or not. Li-ion cell design and run-time thermal management must be carried out to either reduce the numerator or increase the denominator or both in equation (8).

The first eigenvalue μ_1 can be determined by solving the transcendental equation (6) once Biot number, comprising the cell radius, R , thermal conductivity, k_r , and outside convective heat transfer coefficient, h , is known. μ_1 is plotted as a function of the Biot number in Supplementary Fig. 1. As Bi increases, μ_1 increases, but eventually saturates. This means that regardless of how strong convective heat transfer outside the cell is, the value of μ_1 will at most be 2.405. Simply continuing to increase Bi does not necessarily improve the chances of preventing thermal runaway.

Note that equation (8) is derived by assuming the Li-ion cell to be an infinite cylinder, which for most cell geometries such as 18650 and 26650 cells is a reasonable assumption. If a cylinder of finite height H is modeled instead, equation (8) must include additional contributions from the axial eigenvalue as follows:

$$\frac{\beta R^2}{k_r \left(\mu_1^2 + \lambda_1^2 \left(\frac{R}{H} \right)^2 \gamma \right)} < 1 \quad (9)$$

where λ_1 is the first axial eigenvalue, determined based on convective conditions on the top and bottom surfaces, γ is the thermal conductivity ratio k_z/k_r , and H/R is the aspect ratio. As expected, for large aspect ratio, equation (9) reduces to the infinite cylinder result given by equation (8).

A theoretical derivation in Supplementary Information shows that if $Bi \ll 1$, i.e., thermal conduction within the cell is neglected and the entire cell is treated as a lumped thermal mass, as has been done in Semenov plots in previous papers [24,25], equation (8)

reduces to the following simpler form:

$$\beta V < h \cdot A \quad (10)$$

where V and A are the volume and surface area respectively. This corresponds to the Semenov analysis presented in the past that treats the body as a lumped thermal mass. Equation (10) states simply that to prevent thermal runaway, the rate of heat generation must be lower than the rate of heat removal. However, this simplified condition is accurate only for a lumped thermal mass because it does not account for thermal transport within the cell. By accounting for this, the present analysis generalizes the Semenov analysis, and offers a more realistic and accurate prediction of thermal runaway behavior of a Li-ion cell.

The next section discusses experiments carried out on a 26650 thermal test cell to experimentally validate the model presented in this section. Results and discussion are presented in Section 4.

3. Experiments

Experimental investigation of the influence of TRN on thermal runaway presents several challenges. It is difficult to accurately control and measure heat generation rate in a Li-ion cell, particularly one that changes with temperature, as required for such experiments. Further, measurement of temperature inside the cell is not straightforward [14,27]. As a result, these experiments utilize a thermal test cell that mimics heat generation and heat transfer in a Li-ion cell and provides the capability of close control of temperature-dependent heat generation rate.

3.1. Fabrication of thermal test cell

A thermal test cell is designed and built to closely mimic the thermal behavior of a 26650 Li-ion cell. The thermal test cell has similar geometry and thermal transport properties as a 26650 Li-ion cell. Heat generation in the thermal test cell occurs due to Joule heating in a wound resistive metal sheet, which makes it possible to measure and change the heat generation rate as a function of temperature by varying the heating current. A foil of 0.025 mm thick 304 Stainless Steel is first insulated by adhering Kapton tape on its surface. The foil-Kapton sandwich is rolled around a thin rod to form a cylinder of height 65 mm and radius 13 mm. Seven T-type thermocouples are placed during the rolling process at different radii. Thin metal wires are soldered to the two ends of the foil to provide electrical access to the metal foil. The roll is then lowered inside an Aluminum casing of the same dimensions as a 26650 Li-ion cell, and the thin rod is carefully taken out. The heater and thermocouple wires are routed out of the casing. Polydimethylsiloxane (PDMS), a commonly used electrically insulating soft polymer is used to fill any voids in the test cell. PDMS is cured in two steps, for 2 h at 60 °C in each step to remove all air bubbles. Finally, the test cell is sealed with an epoxy.

Thermal conductivity of the thermal test cell is measured to be 0.20 W/mK using an adiabatic radial heating method [29]. This value is close to that of a 26650 Li-ion cell [29,30].

3.2. Temperature-dependent heat generation in thermal test cell

Electrochemical processes in a Li-ion cell generate heat at a rate that typically increases with temperature due to Arrhenius-type nature of these processes [1,3]. In order to obtain a similar temperature dependence of heat generation in the thermal test cell, the heating current, supplied by a LabView-controlled Keithley 2401 sourcemeter is modulated based on temperature measurement from the embedded thermocouples. Fig. 1 shows a picture of the

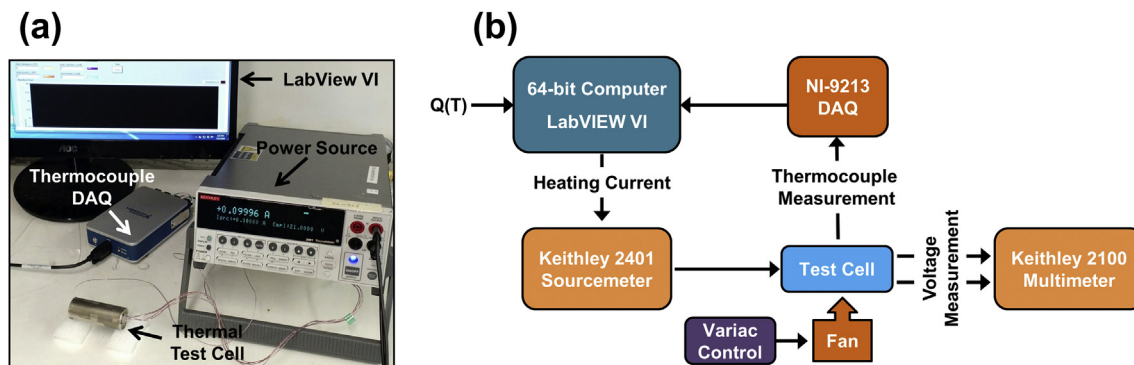


Fig. 1. (a) Picture, and (b) Schematic of the experimental setup.

experimental setup, and a schematic of information flow between various instruments for control of the heat-generation rate. The thermocouple is read every 1 s, and the heating current is changed in order to maintain the heat generation rate according to any desired function of temperature. Simultaneous measurement of heat generation rate is carried out through measurement of input current and induced potential difference. Supplementary Fig. 2 shows that through this feedback, the heat generation rate in the test cell remains close to the desired profile throughout the experiment, thereby demonstrating the capability of producing a desired, temperature-dependent heat generation rate in the thermal test cell. Two specific temperature profiles investigated in this work include linear and Arrhenius-type heat generation as function of temperature.

4. Results and discussion

Supplementary Fig. 3 compares the temperature rise as a function of time predicted by the analytical model in Section 2 with finite-element model simulations, carried out in ANSYS-CFX. This comparison is carried out for linearly increasing heat generation rate at two different values of β , one which is expected to induce

thermal runaway, and one which is not. In both cases, there is good agreement between the analytical model and finite-element simulations.

Fig. 2 plots results from temperature measurements on the thermal test cell subjected to linearly increasing $Q(T)$, with different values of the slope β . Equation (8) predicts that as β increases, the value of TRN will increase, and eventually exceed the threshold value of 1, beyond which thermal runaway is expected to occur. This effect is clearly seen in Fig. 2 where the value of TRN corresponding to various experiments is shown alongside each curve. For low TRN , the cell temperature remains bounded. As TRN increases, the temperature starts to increase due to increased heat generation, but still stays bounded. Once TRN exceeds 1, however, thermal runaway occurs, with the shape of the temperature curve changing from concave to convex. Experimental data in Fig. 2 demonstrate that runaway occurs beyond a threshold value of 1, as expected from the model. In addition, Fig. 2 also shows that in each experiment, there is good agreement between experimental data and analytical model over the entire time period.

As described in section 2, TRN includes contributions from heat generation rate (β), thermal conduction within the cell (k_r) as well as convective heat transfer on the outside (h). To investigate this

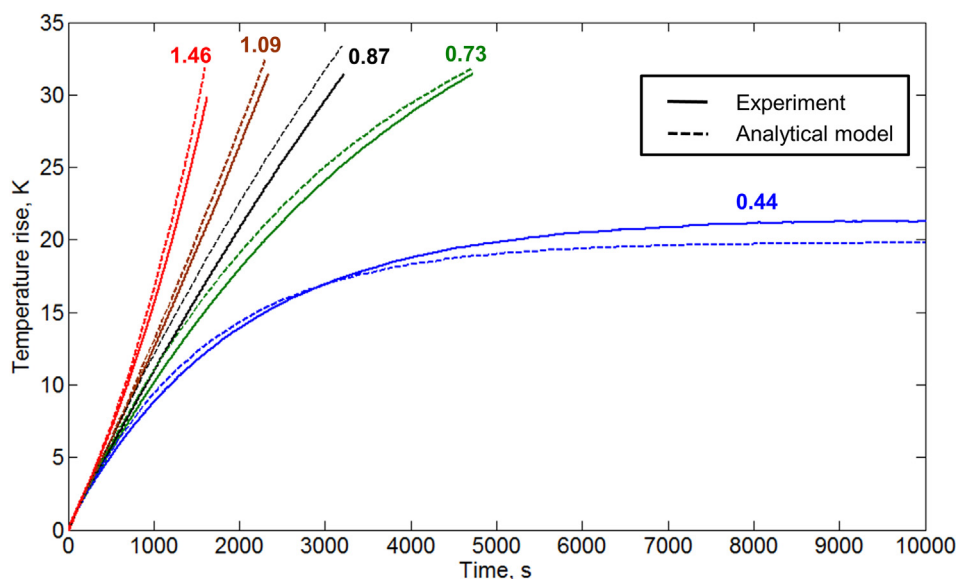


Fig. 2. Core temperature of the thermal test cell measured as a function of time for a number of values of β , ranging from 805 W/m³K for the left-most (blue) curve to 2685 W/m³K for the rightmost (red) curve. These data show that thermal runaway occurs when $TRN > 1$, and is prevented when $TRN < 1$. The value of TRN is shown for each curve. Prediction of temperature profile from the analytical model in Section 2 is also shown for comparison. (For interpretation of the references to colour in this figure legend, the reader is referred to the web version of this article.)

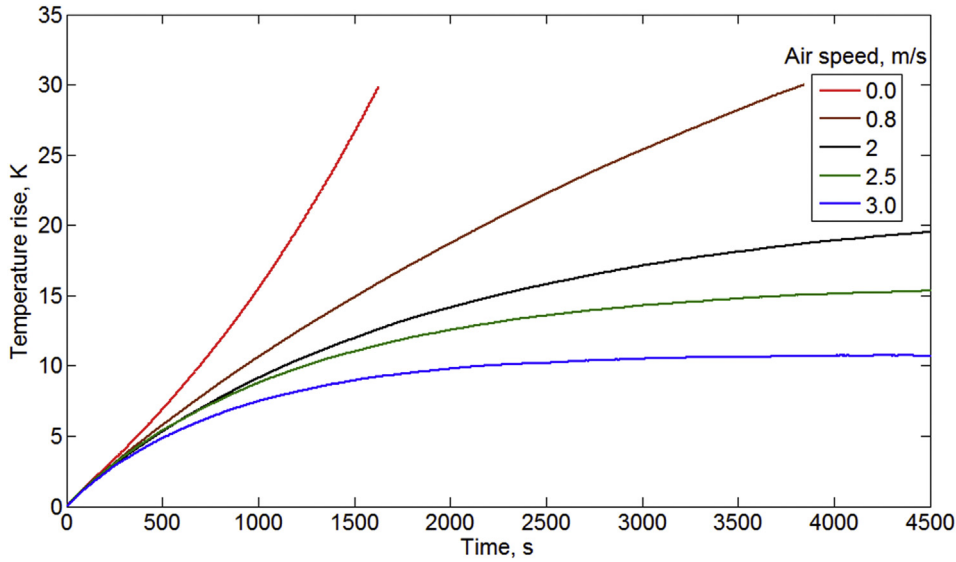


Fig. 3. Core temperature of the thermal test cell measured as a function of time for fixed β and different convective heat transfer conditions.

further, experiments are carried out at fixed β and k_r , but with different cooling conditions on the outside surface of the cell to vary h . This is accomplished by providing a cooling fan to blow air over the fan and varying the cooling air speed. Fig. 3 plots the temperature of the cell as a function of time for these experiments. As the air speed increases, so does h , resulting in reduction in the value of TRN according to equation (8). Eventually, as TRN keeps reducing, as predicted by the model, the cell does not enter into thermal runaway, shown by the bottom three curves in Fig. 3. These data further validate the theoretical prediction of a threshold value of TRN to induce thermal runaway in the cell.

A set of experiments are then carried out using an Arrhenius-type temperature dependence of the heat generation rate, which is more representative of physiochemical processes in a Li-ion cell that are responsible for thermal runaway [32]. In general, the Arrhenius relationship for heat generation rate in a process is given by R.

$$Q(T) = Q_0 \exp\left(-\frac{E_a}{R_u T}\right) \quad (11)$$

where Q_0 is the pre-exponential constant, R_u is the ideal gas constant, and E_a is the activation energy. Note that due to the

exponential relationship, β , the slope of Q is not constant, but increases with increasing temperature.

Two experiments are carried out at two different values of E_a . The values of E_a are chosen such that the resulting TRN corresponding to one of the E_a values crosses over the threshold within a specific temperature window, but not for the other. Fig. 4(a) plots the measured temperature response as a function of time for both cases. As temperature increases, the heat generation rate increases exponentially, which results in a dynamic value of TRN . The variation in TRN as a function of time is also plotted in Fig. 4(a), which shows that for the higher E_a case, TRN always stays under 1, and as a result, the measured temperature remains bounded. For the lower E_a case, TRN starts at a low value, but increases rapidly, and exceeds the threshold of 1 beyond around 1000s. During the time that TRN remains under 1, the temperature profile for this case also appears to remain bounded, but, as expected from the theoretical model, once TRN exceeds 1, the temperature distribution becomes unbounded, resulting in thermal runaway. There is an inflexion in the temperature curve at the time that TRN crosses the threshold value of 1. Fig. 4(b) investigates this further by plotting the temperature profile for the lower E_a value at which thermal runaway occurred in the previous experiment, but with two different cooling conditions

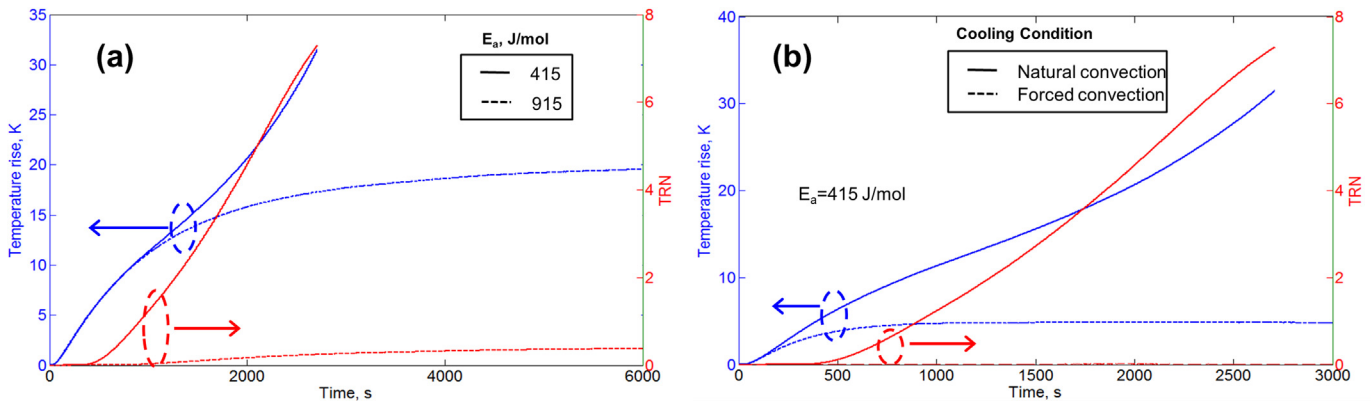


Fig. 4. Experimental measurement of thermal test cell core temperature for (a) two different values of activation energy, E_a , (b) two different values of convective heat transfer coefficient. Plots also indicate the evolution of TRN with time, and show that thermal runaway occurs when TRN exceeds 1.

– natural convection and forced convection using a fan. Fig. 4(b) shows that thermal runaway that occurred in the previous experiment could be prevented through external cooling, which increases the value of h , and hence reduces the value of TRN . Fig. 4(b) shows that when externally cooled, the value of TRN always stays below 1, thereby preventing thermal runaway as predicted by the model presented in section 2.

For a Li-ion cell of a given chemistry and operating at a certain C-rate, there are two thermal transport parameters that influence the rate of heat removal from the cell – the thermal conductivity k_r , which governs the thermal conduction process within the cell, and convective heat transfer coefficient h , which governs heat removal from the cell surface to a coolant through thermal convection. It is important to understand how the value of TRN depends on these two parameters. Fig. 5 shows a colorplot of TRN in the h - k_r space relevant for most practical cooling strategies for $\beta = 6000 \text{ W/m}^3\text{K}$. A curve corresponding to $TRN = 1$, which is the threshold that separates the safe region (to the top and right of the $TRN = 1$ curve) and unsafe region (to the bottom and left of the curve) of this space is also shown. This curve provides a useful design guideline for thermal management of Li-ion cells by specifying what values of thermal transport parameters are expected to be sufficient to prevent thermal runaway at a given value of β . Further, in case thermal runaway is to be expected, this figure shows what parameters need to be changed and by how much in order to cross into the safe region of the h - k_r space shown in Fig. 5. In general, the $TRN = 1$ curve that separates the safe and unsafe regions shifts towards the top and right as β increases, leaving lesser and lesser of the h - k_r space in the safe region. For reference, recent measurements have reported the radial thermal conductivity of 26650 cells to be in the range of 0.2–0.65 W/mK [29,30]. On the h axis, natural convection cooling results in a value of h in the range of 10–100 W/m²K [28], while forced convection values for h are larger, depending on the nature of coolant fluid and flow speed [28].

Fig. 6(a) and (b) plot TRN as a function of h and k_r respectively while the other parameter is fixed. Both figures use $\beta = 6000 \text{ W/m}^3\text{K}$. Fig. 6(a) shows that at a fixed $k_r = 0.2 \text{ W/mK}$, TRN reduces as h increases, i.e., as the cell is cooled more and more aggressively, and dips below the threshold value of 1 at around $h = 233 \text{ W/m}^2\text{K}$. This transition can be made to occur at a lower h , if the thermal

conductivity of the cell could be improved. At $k_r = 1 \text{ W/mK}$, Fig. 6(a) shows that a heat transfer coefficient of 45 W/m²K is sufficient to prevent thermal runaway. Similarly, Fig. 6(b) shows that increasing the cell thermal conductivity reduces TRN when h is held constant. Both Fig. 6(a) and (b) exhibit a saturation effect in TRN as either h or k_r continue to increase. TRN for a cell with too low thermal conductivity might not dip below the threshold value of 1 at all regardless of how effectively it is cooled on the outside. Note that increasing h requires improved heat transfer external to the cell, whereas increasing k_r requires improving material and interfacial thermal resistances within the cell [33].

The interplay between h and k_r for reducing TRN and preventing thermal runaway is further illustrated in Supplementary Fig. 1, which plots the first root μ_1 of equation (6) as a function of the Biot number, Bi . As Bi increases, there is a sharp increase in μ_1 , resulting in significant benefit to TRN , but beyond a value of around 30, further increase in Bi does not significantly increase μ_1 . This illustrates the inherent limitations in using convective cooling to improve thermal runaway performance of the cell, for which k_r is a constant. Once the heat transfer coefficient is somewhat large, its role in preventing thermal runaway saturates, and further benefit must come from thermal-friendly cell design, for example by improving thermal transport through materials and interfaces inside the cell.

When carrying out an effective thermal design of the cell to prevent thermal runaway, parameters such as cell radius and thermal conductivity of the cell are usually fixed, whereas the convective heat transfer coefficient can be increased somewhat, for example, by provided additional coolant flow on the outside of the cell. In such a case, it is important to determine h_{\min} , the minimum value of the convective heat transfer coefficient that can sustain a given heat generation rate without causing thermal runaway. Fig. 7 plots h_{\min} as a function of β for a number of values of the cell thermal conductivity, k_r . This plot shows that for a given value of k_r , as β increases, the minimum value of h needed to prevent thermal runaway increases slowly at first, but then very sharply, eventually becoming too large to be practicable. Since μ_1 has a theoretical maximum value of 2.405 (see Suppl. Fig 3), therefore, for a given R and k_r , the maximum β that a cell can sustain without thermal runaway is given by $\beta_{\max} = 5.78 \cdot k_r / R^2$, which requires very strong

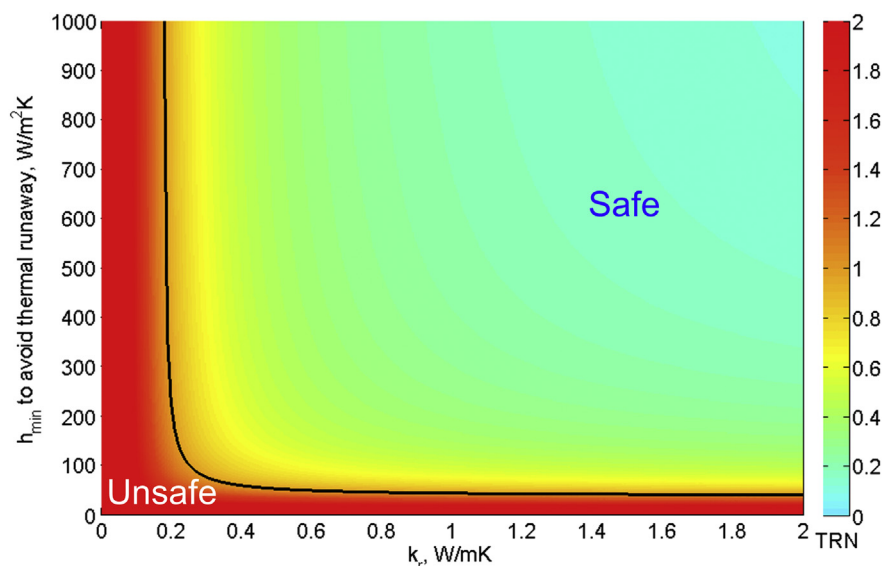


Fig. 5. Colorplot of TRN in the h - k_r space. The $TRN = 1$ curve that separates safe and unsafe regions is also shown.

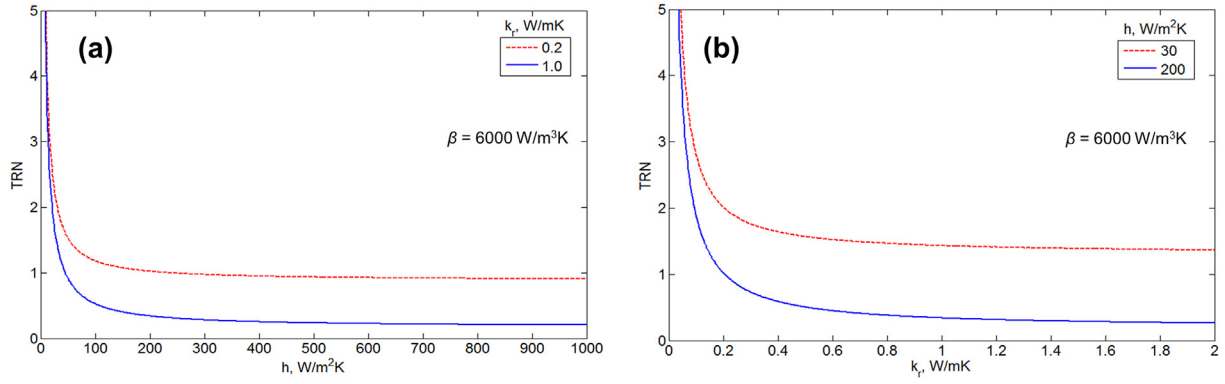


Fig. 6. (a) TRN as a function of the convective heat transfer coefficient, h for two different value of cell thermal conductivity, k_r ; (b) TRN as a function of cell thermal conductivity, k_r , for two different values of heat transfer coefficient, h .

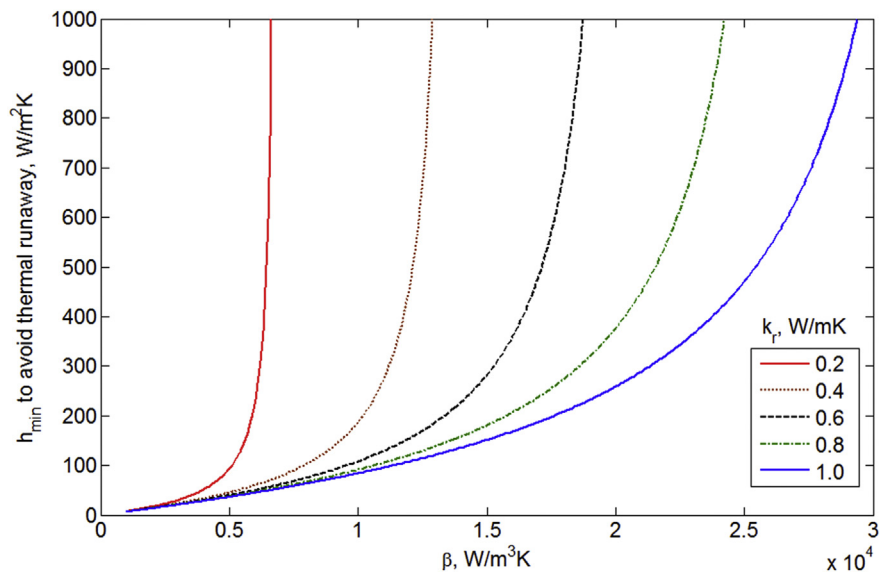


Fig. 7. Minimum heat transfer coefficient needed to prevent thermal runaway as a function of β for different values of cell thermal conductivity.

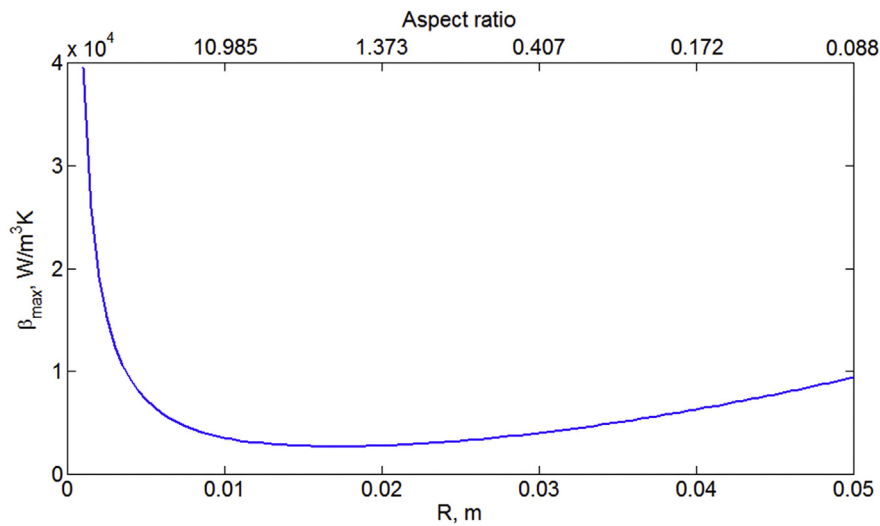


Fig. 8. Maximum sustainable β as a function of the aspect ratio of a finite-length, cylindrical cell.

convective cooling corresponding to a Biot number of around 50 or more. If the expected β of a cell is greater than β_{\max} , then even the best possible external cooling may not be effective.

Finally, the two-dimensional thermal runaway model is utilized to predict β_{\max} , the maximum value of β that a cell can sustain as a function of the shape of the cell. Fig. 8 plots β_{\max} as a function of cell radius for fixed total volume, corresponding to the volume of a 26650 cell. As R increases, β_{\max} first reduces, but then starts increasing after reaching a minima. This non-monotonic behavior occurs because for a fixed volume, equation (9) can be rearranged as follows:

$$\beta_{\max} = k_r \left(\frac{\mu_1^2}{R^2} + \frac{\lambda_1^2 \gamma \pi^2 R^4}{V^2} \right) \quad (12)$$

where V is the volume.

The first term in equation (12) is inversely proportional to R^2 , whereas the second term is directly proportional to R^4 , which explains the non-monotonic behavior in Fig. 8. This shows that among all cells of the same volume at given values of h and k , the cell of a certain radius sustains the lowest β_{\max} , and thus has the worst possible thermal runaway behavior at the assumed values of h and k_r . This worst-case radius can be easily obtained by differentiating equation (12). For conditions considered here, as shown in Fig. 8, this minima occurs at a radius of around 17 mm, which is quite close to that of the commonly used 26650 cell.

5. Conclusions

Thermal runaway is a serious technological challenge that currently limits performance of energy storage and conversion devices. This work experimentally and theoretically demonstrates a new non-dimensional Thermal Runaway Number, TRN , that determines whether thermal runaway will occur or not. In addition to improving the fundamental understanding of heat transfer in thermal runaway conditions, this work contributes towards the design of effective thermal management strategies for preventing thermal runaway and for proactively predicting thermal runaway. By quantifying the limits on heat generation rate in given thermal conditions, this work may also contribute towards the design of resilient cell chemistries that better withstand thermal runaway in unfavorable thermal conditions.

Acknowledgments

This material is based upon work supported by CAREER Award No. CBET-1554183 from the National Science Foundation.

Appendix A. Supplementary data

Supplementary data related to this article can be found at <http://dx.doi.org/10.1016/j.jpowsour.2016.08.133>.

References

- [1] Q. Wang, P. Ping, X. Zhao, G. Chu, J. Sun, C. Chen, J. Power Sources 208 (2012) 210–224.
- [2] D. Lisbona, T. Snee, Process Saf. Env. Prot. 89 (2011) 434–442.
- [3] R. Spotnitz, J. Franklin, J. Power Sources 113 (2003) 81–100.
- [4] P.G. Balakrishnan, R. Ramesh, J. Power Sources 155 (2006) 401–414.
- [5] E.P. Roth, D.H. Doughty, J. Power Sources 128 (2004) 308–318.
- [6] M.N. Richard, J.R. Dahn, J. Electrochem. Soc. 146 (1999) 2068.
- [7] H. Maleki, G. Deng, A. Anani, J. Howard, J. Electrochem. Soc. 146 (1999) 3224–3229.
- [8] A. Du Pasquier, F. Disma, T. Bowmer, A.S. Gozdz, G. Amatucci, J.-M. Tarascon, J. Electrochem. Soc. 145 (1998) 472–477.
- [9] D. Aurbach, B. Markovsky, G. Salitra, E. Markevich, Y. Talyossef, M. Koltypin, L. Nazar, B. Ellis, D. Kovacheva, J. Power Sources 165 (2007) 491–499.
- [10] P. Biensan, B. Simon, J.P. Peres, A. de Guibert, M. Broussely, J.M. Bodet, F. Pertion, J. Power Sources 82 (1999) 906–912.
- [11] E.P. Roth, G. Nagasubramanian, Thermal Stability of Electrodes in Li-ion Cells, Technical Report SAND2000–0345J, Sandia National Laboratories, USA, 2000.
- [12] Y. Chen, J.W. Evans, J. Electrochem. Soc. 143 (1996) 2708–2712.
- [13] Z. Zhang, D. Fouchard, J.R. Rea, J. Power Sources 70 (1998) 16–20.
- [14] S. Drake, M. Martin, D.A. Wetz, J.K. Ostanek, S.P. Miller, J.M. Heinzel, A. Jain, J. Power Sources 285 (2015) 266–273.
- [15] Y. Ye, L.H. Saw, Y. Shi, K. Somasundaram, A.A.O. Tay, Electrochim. Acta 134 (2014) 327–337.
- [16] G.-H. Kim, A. Pesaran, R. Spotnitz, J. Power Sources 170 (2007) 476–489.
- [17] N. Tanaka, W.G. Bessler, Solid State Ion. 262 (2014) 70–73.
- [18] M.W. Verbrugge, AlChE J. 41 (1995) 1550–1592.
- [19] C.F. Lopez, J.A. Jeevarajan, P.P. Mukherjee, J. Electrochem. Soc. 162 (2015) A2163–A2173.
- [20] K. Smith, G.-H. Kim, E. Darcy, A. Pesaran, Int. J. Energy. Res. 34 (2010) 204–215.
- [21] S. Al Hallaj, H. Maleki, J.S. Hong, J.R. Selman, J. Power Sources 83 (1999) 1–8.
- [22] K. Shah, S.J. Drake, D.A. Wetz, J.K. Ostanek, S.P. Miller, J.M. Heinzel, A. Jain, J. Power Sources 258 (2014) 374–381.
- [23] K. Shah, S.J. Drake, D.A. Wetz, J.K. Ostanek, S.P. Miller, J.M. Heinzel, A. Jain, J. Power Sources 271 (2014) 262–268.
- [24] N.N. Semenov, Some Problems in Chemical Kinetics and Reactivity vol. 2, Princeton University Press, 1959. Chap. 8.
- [25] Q. Wang, J. Sun, G. Chu, Proceedings of 8th International Symposium in Fire Safety Science, 2005, pp. 375–382.
- [26] S. Drake, M. Martin, D.A. Wetz, J.K. Ostanek, S.P. Miller, J.M. Heinzel, A. Jain, J. Power Sources 285 (2015) 266–273.
- [27] G. Zhang, L. Cao, S. Ge, C.-Y. Wang, C.E. Shaffer, C.D. Rahn, J. Electrochem. Soc. 161 (2014) A1499–A1507.
- [28] F.P. Incropera, D.P. Dewitt, Introduction to Heat Transfer, 3rd. Ed., Wiley Inc., 2006.
- [29] S.J. Drake, D.A. Wetz, J.K. Ostanek, S.P. Miller, J.M. Heinzel, A. Jain, J. Power Sources 252 (2014) 298–304.
- [30] J. Zhang, B. Wu, Z. Li, J. Huang, J. Power Sources 259 (2014) 106–116.
- [31] M.N. Özisik, Heat Conduction, second ed., John Wiley & Sons Inc, 1980, ISBN 0-471-05481-X.
- [32] V. Srinivasan, C.Y. Wang, J. Electrochem. Soc. 150 (2003) A98–A106.
- [33] V. Vishwakarma, C. Waghela, Z. Wei, R.S. Prasher, S.G. Nagpure, J. Li, F. Liu, C. Daniel, A. Jain, J. Power Sources 300 (2015) 123–131.